

Real-Time Spatial Trajectory Planning for Urban Environments Using Dynamic Optimization

Jona Ruof, Max Bastian Mertens, Michael Buchholz, and Klaus Dietmayer
Institute of Measurement, Control, and Microtechnology, Ulm University, Germany
 {firstname}.{lastname}@uni-ulm.de

arXiv:2305.02621v2 [cs.RO] 9 Aug 2023

Abstract—Planning trajectories for automated vehicles in urban environments requires methods with high generality, long planning horizons, and fast update rates. Using a path-velocity decomposition, we contribute a novel planning framework, which generates foresighted trajectories and can handle a wide variety of state and control constraints effectively. In contrast to related work, the proposed optimal control problems are formulated over space rather than time. This spatial formulation decouples environmental constraints from the optimization variables, which allows the application of simple, yet efficient shooting methods. To this end, we present a tailored solution strategy based on ILQR, in the Augmented Lagrangian framework, to rapidly minimize the trajectory objective costs, even under infeasible initial solutions. Evaluations in simulation and on a full-sized automated vehicle in real-world urban traffic show the real-time capability and versatility of the proposed approach.

Index Terms—trajectory planning, automated driving, augmented lagrangian, iterative lqr

I. INTRODUCTION

Trajectory planning forms the foundation for numerous applications in automated driving. Recently, the development has been increasingly focused on planning in urban environments [1], [2], [3]. This has proven challenging, as the interdependence between traffic participants and the resulting problem complexity often make situations hard to predict. In order to still react safely in critical situations, trajectory updates need to be computed with high frequency. Additionally, the situational diversity of urban traffic imposes varied space, velocity, acceleration, or even spatiotemporal constraints, making methods with high generality necessary. Moreover, the comfort and safety of the resulting trajectory are often directly dependent on the considered horizon. Computing foresighted trajectories thereby requires planning over intervals > 10 s or often up to the perception range of the vehicle (> 100 m). The requirement of generality combined with long-horizon planning contradicts fast reaction times, thus constituting a conflict that needs to be addressed.

Towards the outlined dilemma, we investigate the formulation of a trajectory planning framework, which is designed to run at high frequencies (e.g. 100 Hz) and is versatile enough to handle driving in urban environments. In contrast to

Part of this work has been financially supported by the Federal Ministry for Economic Affairs and Climate Action of Germany within the program “Highly and Fully Automated Driving in Demanding Driving Situations” (project LUKAS, grant number 19A20004F).

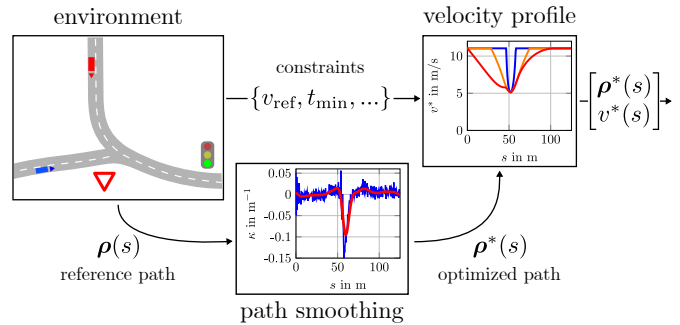


Fig. 1. Overview of the proposed approach given an exemplary urban scenario. The ego vehicle (blue) has to reach a traffic light in time while respecting the right of way of the other vehicle (red). We propose a spatial, decomposed path-velocity formulation (Sec. III) which is solved with a dynamic optimization approach (Sec. IV).

most related work, we explore the optimization of trajectories over *space* rather than *time*. This choice is motivated by the observation that in automated driving, many situations (e.g. speed limits, stop signs, traffic lights, ...) impose constraints expressed as functions of space s . By defining the trajectory likewise as a function of space, the constraint value is decoupled from the resulting state $x(s)$ and control variables $u(s)$ in the trajectory. This is in contrast to a temporal formulation, where, e.g., $s(t = 10\text{ s})$ at the end of the trajectory is dependent on the choice of the acceleration $a(t = 0\text{ s})$ at the beginning of the trajectory. For locally fixed constraints, the spatial formulation stabilizes the optimization, even permitting the use of efficient single-shooting methods (such as AL-ILQR), which are often considered less practical for longer time horizons [4].

Structurally, we propose to apply a path-velocity decomposition approach (Fig. 1), where this work is focused on longitudinal optimization. Our main contributions are:

- A dynamic optimization formulation, which can be solved in the millisecond range (< 10 ms) and generates foresighted trajectories over a 125 m horizon. Additionally, static and dynamic obstacles, velocity, acceleration, curvature limits, as well as spatiotemporal constraints, are considered.
- A tailored, real-time capable solution strategy based on ILQR in the Augmented Lagrangian framework, with improved optimization stability and implicit treatment of

infeasible initializations.

- An evaluation in simulation and on a full-sized automated vehicle in real urban traffic, demonstrating the versatility and robustness of the presented approach.
- An open-source implementation in C and Python along with simulated experiments, which can be found at <https://github.com/joruof/tpl>.

The remainder of this paper is structured as follows: after discussing related work in Sec. II, the two central dynamic optimization objectives are presented and motivated in Sec. III. Then the solution strategy is outlined in Sec. IV, and the presented approach is evaluated in simulation and real-world experiments in Sec. V. We conclude with a brief discussion of current limitations and directions for future work in Sec. VI.

II. RELATED WORK

Literature related to our contribution can be grouped into three main categories, which are discussed in this section.

A. Urban Trajectory Planning Frameworks

While many trajectory planning strategies for vehicles have been developed, most publications focus on specific scenarios and only few propose general methods for urban environments. End-to-end learning methods such as [5] show promising results, but often consider short horizons and exhibit generalization issues. Recently, [1] introduced a general motion planning framework based on Bézier sampling, which was proven effective in real-world scenarios. Ziegler et al. [6] proposed local-continuous optimization to obtain trajectories in a general planning framework, which is able to drive a car on public urban roads. For long horizons, graph search methods in combination with continuous optimization have been demonstrated by Hubmann et al. [7] for longitudinal planning. Our previous work [2], similarly to [6], also relied on continuous optimization supported by driver models and performed well on public urban roads. Another recent work is [3], using local-continuous optimization in an MPC (Model Predictive Control) fashion and showing promising results for overtaking and cut-in scenarios in simulation. In contrast to our work, all listed publications either update the trajectory with lower frequency ([7], [2] @ 10 Hz; [3], [1] @ 20 Hz; [6] terminates after 0.5 s), consider only a short horizon (max. 3 s in [3]), or do not handle explicit spatiotemporal constraints.

B. Iterative LQR

The iterative LQR (ILQR) algorithm [8] is a single-shooting, discrete-time, local-continuous trajectory optimization method. It has been successfully applied to optimal control in various robotic applications, though usually with short horizons for e.g. trajectory tracking [9], [10].

Further ILQR variants have been proposed to handle, e.g., multiple-shooting objectives [4] or control constraints [11]. State constraints have been, e.g., handled in an interior point variant [12] or in a simpler approach called Constrained Iterative LQR (CILQR), proposed in [13] and further analyzed

in [14]. CILQR uses barrier functions to enforce state constraints and has already been successfully applied to automated driving: While initially being developed for obstacle avoidance in [13], it has been extended with stochastic prediction and weight-tuning to handle more diverse situations, such as cut-ins [14]. Moreover, [15] improves numerical issues in CILQR and introduces initial trajectory guesses, while [16] utilizes CILQR for planning with reduced jerk and also explores automatic weight tuning.

While the barrier functions used in CILQR are comparatively simple to understand and implement, they suffer from numerical issues in case of infeasible initialization (cf. [15]) and must be tuned either manually or with an automatic weight-tuning scheme (cf. [16], [14]). Recently, these issues have been addressed by incorporating ILQR in an ADMM (Alternating Direction Method of Multipliers) method [17]. Another numerically robust, but simpler alternative for enforcing constraints is the Augmented Lagrangian (AL) method, as implemented by the ALTRO package [18] as AL-ILQR. Although AL-ILQR strikes a balance between implementation/runtime complexity and constraint satisfaction, it has not yet been adapted for long-horizon trajectory planning in automated driving.

C. Spatial Trajectory Planning

The development of long-horizon, spatial trajectory planning is mainly driven by research in the domain of automated trucking. Earlier works such as [19] already proposed spatial trajectories to compute long-horizon trajectories for reduced fuel consumption and were recently extended in [20]. In contrast to our work, these works obtain trajectories through dynamic programming and also update with much lower rates (e.g., 200 ms in [20]). Another recent work [21] similarly applies a path-velocity decomposition and plans trajectories in the spatial domain. In contrast to our online approach, they solve part of the planning problem offline and do not consider spatiotemporal constraints.

III. FORMULATION

The following section outlines general path and velocity objectives defined over *space* and shows how constraints are represented in the objectives.

A. Path Objective

We assume access to a reference path $\boldsymbol{\rho}(s) = [\hat{x}(s), \hat{y}(s)]^T$ given as a vector-valued function in a 2D Cartesian frame over space s from, e.g., a prerecorded GPS map or a lane detection module. As the path curvature $\kappa(s)$ directly limits the maximum velocity, accurate estimation is crucial for the generation of a smooth velocity profile. Because local curvature computation yields noisy results [22], we adopt the formulation from [22]. Thereby, a path with smoothed curvature is found as a solution to an optimal control problem with state $\mathbf{x}_r = [x_r, y_r, \phi_r]^T$ and control $u_r = \kappa$. The objective dynamics $\partial \mathbf{x}_r / \partial s = \mathbf{f}_r(\mathbf{x}_r, u_r)$ are given by

$$\frac{\partial x_r}{\partial s} = \cos(\phi_r), \quad \frac{\partial y_r}{\partial s} = \sin(\phi_r), \quad \frac{\partial \phi_r}{\partial s} = \kappa, \quad (1)$$

which are integrated from the boundary condition $\mathbf{x}_r(0) = \mathbf{x}_{r,0}$ over space $s \in [0, S]$, with S being the path horizon. Trajectories obtained through the integration are rated by the quadratic function (dropping s for sake of readability)

$$l_r(\mathbf{x}_r, u_r) = w_d \cdot \|(\hat{x} - x_r, \hat{y} - y_r)\|_2^2 + w_\kappa \cdot \|\kappa\|_2^2, \quad (2)$$

with w_d, w_κ being weights on the error of the Cartesian coordinates and the applied curvature, respectively. Including box-constraints $\kappa \in [\kappa_{\min}, \kappa_{\max}]$ to ensure dynamic feasibility, the objective formulates as

$$\min_{\kappa(\cdot)} \int_0^S l_r(\mathbf{x}_r, u_r) ds \quad \text{s.t.} \quad \frac{\partial \mathbf{x}_r}{\partial s_r} = \mathbf{f}_r(\mathbf{x}_r, u_r), \quad (3a)$$

$$\mathbf{x}_r(0) = \mathbf{x}_{r,0}, \quad \kappa_{\min} \leq \kappa \leq \kappa_{\max}. \quad (3b)$$

For a minimizer $\kappa^*(s)$ of the objective, a driveable reference path with smoothed curvature $\rho^*(s)$ is then obtained by the respective integrals of x_r, y_r over s .

B. Velocity Objective

Starting from $a(t) = \partial v / \partial t$, the application of the chain rule allows the definition of velocity over space dynamics

$$a(t) = \frac{\partial v}{\partial t} = \frac{\partial v}{\partial s} \frac{\partial s}{\partial t} = \frac{\partial v}{\partial s} v(t) \quad \Leftrightarrow \quad \frac{\partial v}{\partial s} = \frac{a(t)}{v(t)}. \quad (4)$$

Analogously, spatial dynamics for jerk j and time t are $\partial j / \partial s = j(t) / v(t)$, $\partial t / \partial s = 1 / v(t)$. One obvious problem with this dynamics function is the singularity at $v = 0$. Numerical issues are prevented by limiting $v \geq v_{\min}$, where v_{\min} is some small positive value. Velocities at v_{\min} are set to 0 in a postprocessing step, if the target velocity $v_{\lim} = 0$. In general form, we assume that target/maximum velocities are specified over space as $v_{\lim}(s)$. The generation of $v_{\lim}(s)$ depending on the concrete traffic situation is detailed in the following subsections. From v_{\lim} we generate a reference profile v_{ref} and a velocity profile v^* , as depicted in Fig. 2. This profile generation process is explained now.

As $v_{\lim}(s)$ may not respect jerk or acceleration constraints $[j_{\min}, j_{\max}]$, $[a_{\min}, a_{\max}]$, the constraint profile first is shaped by integrating

$$\left(\frac{\partial v}{\partial s}, \frac{\partial a}{\partial s} \right)^T = \begin{cases} (a/v, j/v)^T & : v \leq v_{\lim} \\ (0, 0)^T & : \text{else} \end{cases} \quad (5)$$

once backwards from horizon S to 0, with $j(s) = j_{\min}$, boundary condition $(v(S), a(S))^T = (v_{\lim}(S), 0)$, and once forwards with $j(s) = j_{\max}$, boundary condition $(v(0), a(0))^T = (v(0), 0)$. Additionally, during integration of the resulting profiles v_{bwd} and v_{fwd} , states v, a are limited after every integration step to $v = \min(v, v_{\lim})$ and $a = \text{clip}(a_{\min}, a_{\max}, a)$. Application of the minimum operator then yields a profile

$$v_{\text{ref}}(s) = \min(v_{\text{bwd}}(s), v_{\text{fwd}}(s)), \quad (6)$$

which respects acceleration and jerk limits, but is neither foresighted nor comfortable. Therefore, v_{ref} is subsequently incorporated into a dynamic optimization objective as a velocity target and as an upper limiting function for feasible profiles.

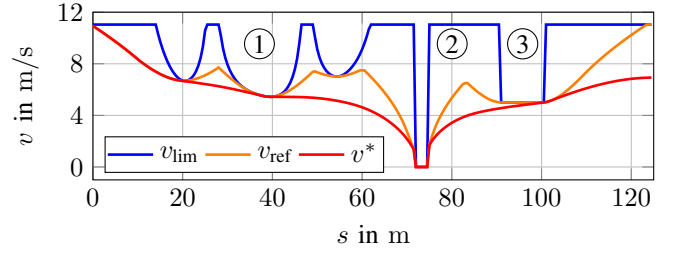


Fig. 2. Intermediate steps of the velocity profile generation: Based on v_{\lim} , an acceleration and jerk limited profile v_{ref} is generated, then optimized to yield a foresighted v^* profile. Marker 1 shows an exemplary velocity constraint through road curvature. Markers 2 and 3 show interaction constraints.

To this end, we define $\mathbf{x}_v = [v, t]^T$, $u_v = a$, and $f_v(\mathbf{x}_v, u_v) = [\partial v / \partial s, \partial t / \partial s]^T$ with boundary condition $v(0) = v_{\text{veh}}$. Profiles $v(s)$ generated by forward integration of $f_v(\mathbf{x}_v, u_v)$ are rated by the quadratic function

$$l_v(\mathbf{x}_v, u_v) = w_v \|v(s) - v_{\text{ref}}(s)\|_2^2 + w_a \|a(s)\|_2^2 \quad (7)$$

with weights w_v, w_a . Combining dynamics f_v and (7) yields a dynamic minimization objective over velocity profiles

$$\min_{a(\cdot)} \int_0^S l_v(\mathbf{x}_v, u_v) ds \quad \text{s.t.} \quad \frac{\partial \mathbf{x}_v}{\partial s} = f_v(\mathbf{x}_v, u_v), \quad (8a)$$

$$v_{\min} \leq v \leq v_{\text{ref}}, \quad a_{\min} \leq a \leq a_{\max}, \quad (8b)$$

where the optimal profile $v^*(s)$ is obtained by the integral of a minimizer a^* of this objective using the dynamics (4).

While the cost function l_v takes a simple quadratic form, the objective becomes intricate through its non-linear dynamics and the presence of control and state constraints (8b). Thus, a specialized algorithm is required to solve the objective efficiently, which we propose in Sec. IV.

C. Speed Limits

In the case of urban automated driving, the velocity limit function $v_{\lim}(s)$ (Fig. 2) is shaped by legal speed limits v_{lg} and implicit velocity limits induced by the curvature $\kappa^*(s)$ of the road. Given a maximum admissible lateral acceleration \hat{a}_{lat} , v_{\lim} is initially given by

$$v_{\lim}(s) = \min \left(v_{\text{lg}}(s), \sqrt{|\hat{a}_{\text{lat}}| / |\kappa^*(s)|} \right), \quad (9)$$

where $\kappa^*(s)$ is obtained as solution of objective (3).

D. Interaction Constraints

Static interaction constraints, which are fixed to a certain location s_o , are expressed simply by updating v_{\lim} with the minimum operator

$$v_{\lim}(s_o) \leftarrow \min(v_{\lim}(s_o), v_o), \quad (10)$$

where $v_o = 0$ for interactions that require stopping (e.g. traffic lights) and $0 \leq v_o \leq v_{\lim}$ for interactions with velocity reductions. Note that through the backward-forward integration presented in (5), even significant changes in v_{\lim} (e.g. through obstacles) still result in a smooth reference profile v_{ref} (Fig. 2).

Similarly to static interactions, we consider generic dynamic interactions (e.g., cars, bicycles, ...) at position s_o with velocity v_o as constraints in the velocity profile. The obstacles are expressed by a reactive velocity constraint formulation, motivated by a constant velocity prediction. Given a safety distance d_{safe} (which may depend on v), the constraint updates v_{lim} according to

$$v_{\text{lim}}(s) \leftarrow \min(v_{\text{lim}}(s), v_o \cdot \min(1, s_o/d_{\text{safe}})), \quad (11)$$

at all $s \in [s_o - d_{\text{safe}}, s_o]$. The resulting velocity constraint ensures that $v = v_o$ at the beginning of the safety distance and then reduces v proportional to the amount of safety distance violation until standstill at $s = s_o$. This heuristic ensures that in case of a decelerating obstacle, the distance is increased and approaches the safety distance, provided the obstacle decelerates no more than a_{min} . Even in case of a slow obstacle ahead, a collision is avoided if there is any viable solution given the same dynamics limits. While this way of handling obstacles may seem simplistic, it results in safe and smooth behavior, assuming fast replanning cycles.

E. Spatiotemporal Constraints

Spatiotemporal constraints (like in Fig. 1) restrict the ego vehicle to a certain time interval at a certain location. Maximum spatiotemporal constraints require that the vehicle reaches a point s at time $t(s) \leq t_{\text{max}}(s)$, which may increase acceleration and velocity. This is always feasible if the velocity stays below v_{ref} and the acceleration within $[a_{\text{min}}, a_{\text{max}}]$. Thus, $t_{\text{max}}(s)$ constraints can be included simply as additional state constraints in objective (8). In contrast, minimum spatiotemporal constraints require that $t(s) \geq t_{\text{min}}(s)$, which may reduce velocity until standstill. Naively applying t_{min} constraints without additional regularization often causes stopping far ahead of the constraint location. While this solution is valid, it is often perceived as unintuitive or obstructive by other traffic participants. Therefore, we propose to express a t_{min} constraint at s_c via the inequality

$$(t_{\text{min}}(s_c) - t(s_c)) \cdot (v(s_c) - v_{\text{min}}) \leq 0. \quad (12)$$

The left side contains the constraint as-is in the first factor but also approaches zero by reducing the velocity to v_{min} in the second factor. Inequality (12) therefore expresses, in a continuous way, that both reducing the time at s_c to t_{min} as well as stopping at s_c lead to constraint satisfaction. Additionally, we replace the weight on the reference velocity deviation w_v in (7) with $w_v(s)$ shaped by

$$w_v(s) = \min(1, ((s - s_c - \alpha) \cdot \beta)^2). \quad (13)$$

For a given offset $\alpha \geq 0$ and scale $0 < \beta < 1$, this weighting function mitigates the conflict between driving at v_{ref} and reducing v , so that $t_{\text{min}}(s_c)$ holds. As the function is minimal at or above s_c , it encourages stopping precisely at s_c . In our experiments, including both (12) and (13) in objective (8) leads to decisive constraint handling behavior, either slowing down before the constraint or stopping precisely at s_c .

Algorithm 1 Solution Strategy

```

initialize  $n \leftarrow 1$  and  $\mu_i$  with fixed large values
initialize  $\mathbf{X}, \mathbf{U}, \boldsymbol{\lambda}$  shifted from previous step
while  $n < N$  and cost change  $>$  tol do
    minimize objective (14) with ILQR iteration
end while
 $\lambda_{k,i} \leftarrow \lambda_{k,i} + \mu_i h_i(\mathbf{x}_k, \mathbf{u}_k)$ 
 $\lambda_{k,i} \leftarrow \max(0, \min(\lambda_{k,i}, \lambda_{\text{max},i}))$ 

```

IV. SOLUTION STRATEGY

The solution strategy is based on ILQR, which is a single-shooting, discrete-time, local-continuous trajectory optimization method for unconstrained dynamic optimization objectives with general non-linear dynamics and cost functions (cf. [8]). We argue that ILQR is a suitable choice for automotive applications as it, firstly, can be implemented efficiently for small control spaces in plain C code (e.g. on embedded devices) even without specialized numeric routines. Secondly, ILQR runtime complexity scales only linearly with the optimization horizon, which makes it suitable for long-horizon planning. Thirdly, being a shooting method, trajectories generated with ILQR are by design always dynamically consistent, even when the optimization is terminated early. This allows one to trade off reaction time for a temporarily suboptimal solution, which is subsequently improved over multiple iterations (for convergence results cf. [23]).

A. Augmented Lagrangian ILQR

As demonstrated by [18], ILQR can be embedded in an Augmented Lagrangian method to solve discretized, constrained dynamic optimization objectives

$$\min_{\mathbf{u}_1, \dots, \mathbf{u}_K} \mathcal{L}(\mathbf{X}, \mathbf{U}, \boldsymbol{\lambda}, \boldsymbol{\mu}) \quad \text{s.t.} \quad \mathbf{x}_{k+1} = f(\mathbf{x}_k, \mathbf{u}_k), \quad (14)$$

$$h_i(\mathbf{x}_k, \mathbf{u}_k) \leq 0, i \in [1, \dots, I], \forall k \in [1, \dots, K],$$

where $\mathbf{X} = (\mathbf{x}_1, \dots, \mathbf{x}_K)$, $\mathbf{U} = (\mathbf{u}_1, \dots, \mathbf{u}_K)$ are matrices of states and controls, $\boldsymbol{\lambda} \in \mathbb{R}^{K \times I}$ is a matrix of Lagrange multiplier estimates, $\boldsymbol{\mu} \in \mathbb{R}^I$ is a vector of barrier weights, f is the dynamics function, h_i are I constraint functions, and k is the summation index up to a horizon K . Further, \mathcal{L} denotes the Lagrangian

$$\mathcal{L}(\mathbf{X}, \mathbf{U}, \boldsymbol{\lambda}, \boldsymbol{\mu}) = \quad (15)$$

$$\sum_{k=1}^K \left[l(\mathbf{x}_k, \mathbf{u}_k) + \sum_{i=1}^I [\lambda_{k,i} h_i(\mathbf{x}_k, \mathbf{u}_k) + \mu_i h_i(\mathbf{x}_k, \mathbf{u}_k)^2] \right],$$

where l is an integral cost. The Augmented Lagrangian ILQR (AL-ILQR) then alternates between solving objective (14) up to a given tolerance with standard ILQR, increasing the Lagrange multipliers by the amount of weighted constraint violation, and monotonically increasing the quadratic barrier weights until the constraints hold within tolerances (cf. [18]).

TABLE I
OBJECTIVE PARAMETERS USED IN EVALUATION

Parameter(s)	Value(s)
v_{\min}	1.0 m/s
$a_{\min}, a_{\max}, \hat{a}_{\text{lat}}$	$\pm 2.5 \text{ m/s}^2, 2.5 \text{ m/s}^2$
j_{\min}, j_{\max}	$\pm 1.5 \text{ m/s}^3$
$\kappa_{\min}, \kappa_{\max}$	$\pm 3.0 \text{ m}^{-1}$
w_d, w_κ, w_v, w_a	1.0, 20.0, 0.1, 1.0
α, β	10.0, $5 \cdot 10^{-3}$

B. AL-ILQR for Automotive Trajectory Planning

The AL-ILQR approach in [18] is focused on robotic applications, where keeping constraint violations small is crucial. When adapting AL-ILQR for automotive trajectory planning, we argue that rather reaction time is critical, while small numerical temporary constraint violations are tolerable. Algorithm 1 lists the adapted solution strategy. Because Alg. 1 is executed at high rate, we found that a single λ update with high initial μ increases constraint satisfaction sufficiently, thus mitigating the need for multiple AL iterations. In summary, we propose the following modifications:

(i) Barrier weights μ_i are initialized with large values and kept constant. This reduces eventual constraint satisfaction but avoids numerical ill-conditioning for very high barrier weights. This also allows using a standard Riccati backward pass and avoids the higher implementation complexity and runtime of the sqrt-LQR backward pass (cf. [18]).

(ii) Lagrange-multipliers $\lambda_{k,i}$ are limited by $\lambda_{k,i} \leq \lambda_{\max,i}$, thus likewise avoiding numerical issues. In many cases, this even allows infeasible initializations to be treated robustly. The violation of constraints resulting from the limited λ is, for our application, preferred over obtaining no solution at all.

(iii) We do not apply solution polishing like in [18], as it trades increased runtime for lower constraint violation. However, in our case, faster updates are preferred.

(iv) Except for the first optimization step, we reinitialize AL-ILQR in MPC fashion with its results from the previous step shifted by the amount of distance the vehicle has passed. Importantly, this also includes λ , which allows the Lagrange multipliers to be preserved between planning steps. This avoids fully recalculating λ in each planning step, hence mitigating the need for multiple AL iterations.

V. RESULTS

To investigate the effectiveness of the proposed approach, we subject it to a simulated as well as a real-world scenario, which showcase typical situations in urban environments.

A. Implementation

The proposed objectives and the solution strategy were implemented in self-contained C code as Python extensions. Derivatives were obtained with symbolic differentiation via the SymPy package. Further processing steps were implemented in Python. We assume usage of a perception stack, which generates the required information for the trajectory planning algorithm. In both scenarios, the reference line $\rho(s)$

Algorithm 2 Real-time Spatial Trajectory Planning

- 1: given ego state, reference line ρ , environment state
- 2: $\rho^* \leftarrow$ minimize objective (3) using Alg. 1
- 3: extract obstacles concerning ρ^*
- 4: convert ρ^*, κ^* , obstacles into constraints $v_{\text{lim}}, t_{\text{min}}, t_{\text{max}}$
- 5: generate v_{ref} (Sec. III-B)
- 6: $v^* \leftarrow$ minimize objective (8) using Alg. 1
- 7: execute (ρ^*, v^*) via low-level controller

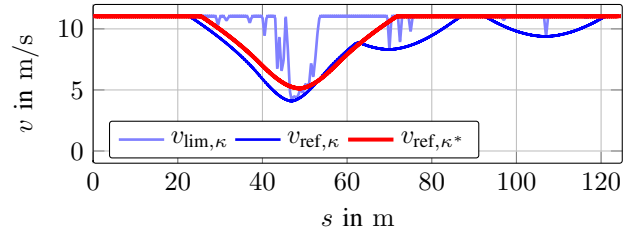


Fig. 3. Effects of the path objective (3): Using local curvature estimates κ leads to noisy v_{lim} and unnecessarily jerky v_{ref} , while κ^* yields a smooth reference profile.

is provided from noisy GPS data recorded on real roads, thus requiring the path optimization from Sec. III-A. All steps of the implementation are summarized in Alg. 2, where the low-level controller is executed with a cycle time of 10 ms. If the runtime of the planning step exceeds 10 ms, the previous solution is executed by the controller. Necessarily, discretization of the integration in the objectives is required. For all scenarios, we use a discrete step size of $\Delta s = 0.5 \text{ m}$ and chose $S = 125 \text{ m}$, which results in 250 spatial steps per objective. Both objective minimizations are terminated if the relative cost change is $< 10^{-6}$ or after $N = 5$ ILQR iterations to preserve real-time feasibility. The barrier weights and multiplier limits $\mu = 10^3, \lambda_{\max} = 10^3$ are used for t_{max} constraints and $\mu = 10^2, \lambda_{\max} = 10^2$ for all other constraints. Further parameters were experimentally determined for comfortable behavior (Table I).

B. Simulated Scenario

The simulated experiments were executed on an AMD 1900X CPU @ 3.8 GHz base clock using a single thread. Perfect knowledge of the states of all vehicles is assumed. The vehicle movement is simulated with a kinematic bicycle model. The complex scenario from Fig. 1 is examined here. Additional scenarios can be found on the project website <https://github.com/joruof/tpl>.

Figure 1 depicts the scenario setup at $t = 0$. The ego vehicle has to merge smoothly onto a main road without stopping while providing right of way to another traffic participant traveling at the speed limit $v_{\text{lg}} = 40 \text{ km/h}$. As an additional complication, a traffic light has to be passed after the intersection, which is scheduled to turn red at $t = 14 \text{ s}$. Figure 3 shows that the path optimization from Sec. III-A leads to accurate curvature estimation and enables the generation of a smooth v_{ref} profile. Given the optimized path, two spatiotemporal

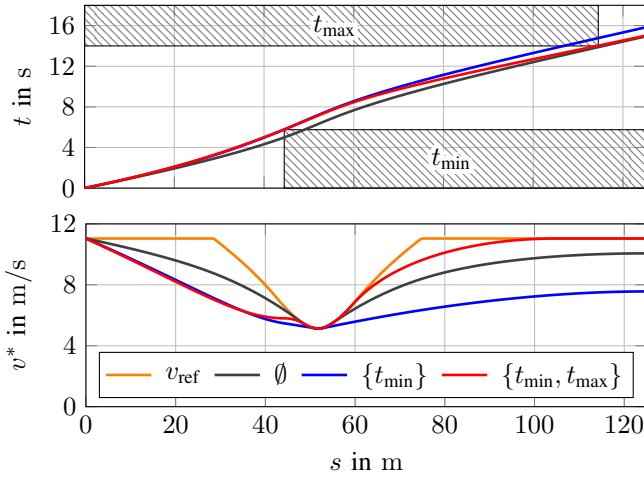


Fig. 4. Resulting velocity profiles at $t = 0$ and driven s - t trajectories for the simulated scenario from Fig. 1, with different spatiotemporal constraints applied (none, only t_{\min} , t_{\min} and t_{\max}). Spatiotemporal constraints are depicted as hatched rectangles.

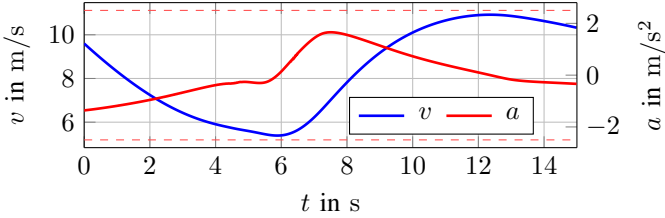


Fig. 5. Velocity and acceleration (with a_{\min} , a_{\max} as dashed lines) of the ego vehicle during the simulated scenario from Fig. 1.

TABLE II

RUNTIMES OF OUR METHOD IN THE SIMULATED SCENARIO FROM FIG. 1.

Component	Mean	Stddev.	Max.
lateral (Eq. (3))	0.354 ms	0.116 ms	1.50 ms
longitudinal (Eq. (8))	0.214 ms	0.101 ms	1.380 ms
total (lat. + lon. + preprocess.)	1.4 ms	0.290 ms	9.610 ms

constraints $t_{\min}(44.5 \text{ m}) = 5.75 \text{ s}$, $t_{\max}(114.5 \text{ m}) = 14.0 \text{ s}$ are generated. Figure 4 compares the resulting velocity profiles for different spatiotemporal constraint sets. Given no spatiotemporal constraints (\emptyset), the intersection is reached too early, resulting in a collision. For $\{t_{\min}\}$ only, the intersection is entered safely, but the green traffic light is missed. With $\{t_{\min}, t_{\max}\}$ applied, a solution is found, which first reduces the velocity at 44.5 m to keep the t_{\min} constraint, then closely follows the reference velocity v_{ref} to reach the traffic light in time. As Fig. 4 and Fig. 5 show, all acceleration, velocity, and spatiotemporal constraints are satisfied by the solution. Runtime statistics for our approach in the simulated scenario are given in Table II. The maximum total runtime for the proposed method, which includes preprocessing, is below 10 ms. The results show that with the proposed method even multiple conflicting constraints can be handled robustly and efficiently.

C. Real World Scenario

The real-world scenario was performed with an automated test vehicle of our institute, a Mercedes-Benz S-Class equipped

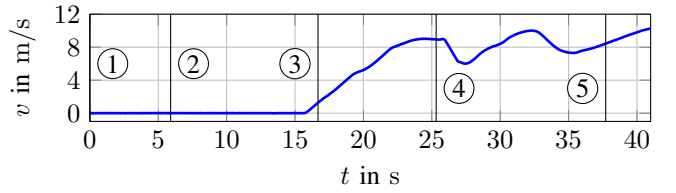


Fig. 6. Vehicle velocity during the real-world scenario. Events 1-5 are marked by numbers and detailed in Fig. 7.

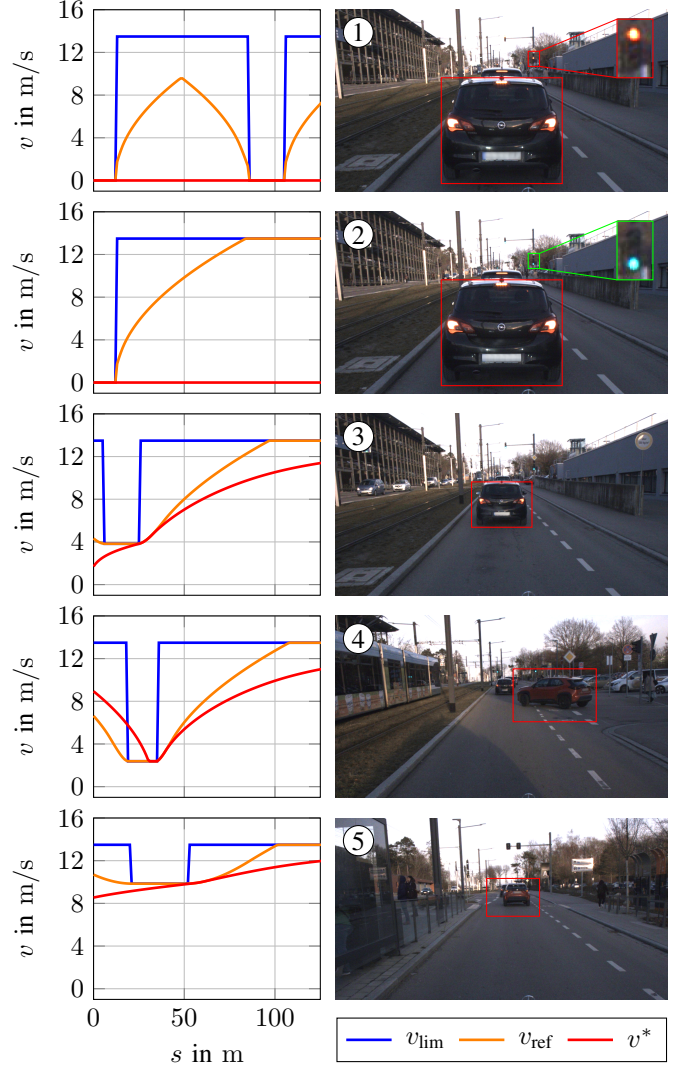


Fig. 7. The left column shows the results of the velocity profile optimization for events 1-5 (Fig. 6) during the real-world scenario, where $s = 0$ is the respective current position of the ego vehicle. For reference, the right column depicts images from the front camera of the ego vehicle, where relevant objects are marked by boxes.

with additional sensors (e.g. cameras, LiDARs). Steering and brake actuators as well as the drive train are controlled by our planning approach. The vehicle state was obtained by a DGPS unit with centimeter accuracy. All computations are performed by an onboard PC with an AMD 3990X CPU @ 2.9 GHz base clock, using a single thread for our planner.

TABLE III
RUNTIMES OF THE PLANNER IN THE REAL-WORLD SCENARIO.

Component	Mean	Stddev.	Max.
lateral (Eq. (3))	0.529 ms	0.195 ms	1.371 ms
longitudinal (Eq. (8))	0.924 ms	0.335 ms	2.371 ms
total (lat. + lon. + preproc.)	6.796 ms	1.627 ms	14.15 ms

As real-world scenario, planning in a dense urban environment is demonstrated. The ego vehicle has to follow a reference line while reacting to the environment and other traffic participants. Figure 6 shows the recorded vehicle velocity, where 5 events are marked. The corresponding velocity profiles for the events of the vehicle are shown together with front camera images in Fig. 7.

Event 1: Initially, the ego vehicle is stopped behind another car, waiting in front of a red light. The resulting velocity profile shows two sections with 0 velocity, corresponding to the leading vehicle and the traffic light.

Event 2: At $t = 5.9$ s, the traffic light turns green, which removes the second section of $v = 0$. As the leading vehicle has not started moving yet, the velocity is still 0 at the beginning of the velocity profile.

Event 3: As the leading vehicle starts moving, the $v \leq v_{\text{ref}}$ constraint is successively lifted, which allows the optimization to increase the velocity, yielding smooth following behavior.

Event 4: A car unexpectedly cuts in front of the ego vehicle, which makes the solution fall below the safety distance thus violating the velocity constraints. In such situations, barrier function constraints [13] quickly raise costs to very large (or undefined) values making the optimization numerically unstable [14]. Due to the proposed limitations of λ , μ , our adapted solution strategy (cf. Sec. IV) remains numerically stable and is able to react adequately. The solution v^* applies minimum acceleration until the constraint is fulfilled while keeping the remainder of the trajectory consistent.

Event 5: After the cut-in, the ego vehicle continues following the leading vehicle normally until the end of the scenario.

Table III lists the runtimes of our method recorded during the real-world scenario. Due to a higher number of objects that need to be preprocessed, the total computation time is higher compared to the simulated scenario, exceeding 10 ms at the maximum. Still, 97.4% of planning steps take less than 10 ms, showing that our approach can rapidly provide trajectory updates, even in complicated real-world scenarios.

VI. CONCLUSION

We have presented a dynamic optimization approach for foresighted trajectory planning, which can handle general velocity as well as spatiotemporal constraints. By choosing a spatial formulation, a fast, tailored AL-ILQR method could be applied, resulting in small cycle times and thus substantially reduced reaction time in complex urban environments. Since the proposed formulation currently plans longitudinally along a provided reference line, future work will focus on extensions that allow for lateral deviations (e.g. for overtaking) and further reduction of the maximum computation time.

REFERENCES

- [1] A. Artunedo, J. Villagra, and J. Godoy, "Real-time motion planning approach for automated driving in urban environments," *IEEE Access*, vol. 7, pp. 180039–180053, 2019.
- [2] M. J. Graf, O. M. Speidel, J. O. Ruof, and K. Dietmayer, "On-road motion planning for automated vehicles at ulm university," *IEEE Intell. Transp. Syst. Magazine*, vol. 14, pp. 121–131, 2022.
- [3] F. Micheli, M. Bersani, S. Arrigoni, F. Braghin, and F. Cheli, "Nmpc trajectory planner for urban autonomous driving," *Veh. System Dynamics*, pp. 1–23, 2022.
- [4] M. Giffthaler, M. Neunert, M. Stauble, J. Buchli, and M. Diehl, "A family of iterative gauss-newton shooting methods for nonlinear optimal control," *IEEE Int. Conf. on Intell. Robots and Syst.*, pp. 6903–6910, 2018.
- [5] S. Casas, A. Sadat, and R. Urtasun, "Mp3: A unified model to map, perceive, predict and plan," in *Proc. of the IEEE/CVF Conf. on Computer Vision and Pattern Recognition*, pp. 14403–14412, 2021.
- [6] J. Ziegler, P. Bender, T. Dang, and C. Stiller, "Trajectory planning for bertha - a local, continuous method," *IEEE Intell. Veh. Symp., Proc.*, pp. 450–457, 2014.
- [7] C. Hubmann, M. Aeberhard, and C. Stiller, "A generic driving strategy for urban environments," *IEEE Conf. on Intell. Transp. Syst., Proc.*, pp. 1010–1016, 2016.
- [8] Y. Tassa, T. Erez, and E. Todorov, "Synthesis and stabilization of complex behaviors through online trajectory optimization," *IEEE Int. Conf. on Intell. Robots and Syst.*, pp. 4906–4913, 2012.
- [9] A. Nagariya and S. Saripalli, "An iterative lqr controller for off-road and on-road vehicles using a neural network dynamics model," *IEEE Intell. Veh. Symp., Proc.*, pp. 1740–1745, 2020.
- [10] J. Chen, C. Liu, and M. Tomizuka, "Foad: Fast optimization-based autonomous driving motion planner," *Proc. of the American Control Conf.*, vol. 6, pp. 4725–4732, 2018.
- [11] Y. Tassa, N. Mansard, and E. Todorov, "Control-limited differential dynamic programming," *IEEE Int. Conf. on Robotics and Automation, Proc.*, pp. 1168–1175, 2014.
- [12] A. Pavlov, I. Shames, and C. Manzie, "Interior point differential dynamic programming," *IEEE Transactions on Control Syst. Technol.*, vol. 29, pp. 2720–2727, 2021.
- [13] J. Chen, W. Zhan, and M. Tomizuka, "Constrained iterative lqr for on-road autonomous driving motion planning," *IEEE Conf. on Intell. Transp. Syst., Proc.*, vol. 3, pp. 1–7, 2018.
- [14] J. Chen, W. Zhan, and M. Tomizuka, "Autonomous driving motion planning with constrained iterative lqr," *IEEE Transactions on Intell. Veh.*, vol. 4, pp. 244–254, 2019.
- [15] Y. Shimizu, S. Kato, W. Zhan, L. Sun, J. Chen, and M. Tomizuka, "Motion planning for autonomous driving with extended constrained iterative lqr," *Dynamic Syst. and Control Conf.*, vol. 1, 2021.
- [16] O. Jahanmahir, Q. Lin, Y. Pan, and J. M. Dolan, "Jerk-minimized cilqr for human-like driving on two-lane roadway," *IEEE Intell. Veh. Symp., Proc.*, vol. 7, pp. 1282–1289, 2021.
- [17] J. Ma, Z. Cheng, X. Zhang, M. Tomizuka, and T. H. Lee, "Alternating direction method of multipliers for constrained iterative lqr in autonomous driving," *IEEE Transactions on Intell. Transp. Syst.*, pp. 1–12, 2022.
- [18] T. A. Howell, B. E. Jackson, and Z. Manchester, "Altro: A fast solver for constrained trajectory optimization," *IEEE Int. Conf. on Intell. Robots and Syst.*, pp. 7674–7679, 2019.
- [19] E. Hellström, M. Ivarsson, J. Åslund, and L. Nielsen, "Look-ahead control for heavy trucks to minimize trip time and fuel consumption," *Control Engineering Practice*, vol. 17, pp. 245–254, 2009.
- [20] S. Bae, Y. Kim, J. Guanetti, F. Borrelli, and S. Moura, "Design and implementation of ecological adaptive cruise control for autonomous driving with communication to traffic lights," *Proc. of the American Control Conf.*, pp. 4628–4634, 7 2019.
- [21] R. Voswinkel, I. Mutlu, K. Alaa, and F. Schrodell, "A modular and model-free trajectory planning strategy for automated driving," *Eur. Control Conf.*, pp. 1186–1191, 2020.
- [22] F. Gritschneider, K. Graichen, and K. Dietmayer, "Fast trajectory planning for automated vehicles using gradient-based nonlinear model predictive control," *IEEE Int. Conf. on Intell. Robots and Syst.*, pp. 7369–7374, 2018.
- [23] K. Graichen and A. Kugi, "Stability and incremental improvement of suboptimal mpc without terminal constraints," *IEEE Transactions on Automatic Control*, vol. 55, pp. 2576–2580, 2010.